

# A tale of two populations: surviving and destroyed dwarf galaxies and the build up of the Milky Way's stellar halo

Azadeh Fattahi<sup>1</sup>\*, Alis J. Deason<sup>1</sup>, Carlos S. Frenk<sup>1</sup>, Christine M. Simpson<sup>2,3</sup>, Facundo A. Gómez<sup>4,5</sup>, Robert J. J. Grand<sup>6</sup>, Antonela Monachesi<sup>4,5</sup>, Federico Marinacci<sup>7</sup>, Rüdiger Pakmor<sup>6</sup>

<sup>1</sup> Institute for Computational Cosmology, Department of Physics, University of Durham, South Road, Durham DH1 3LE, UK

<sup>2</sup> Enrico Fermi Institute, The University of Chicago, Chicago, IL 60637, USA

<sup>3</sup> Department of Astronomy & Astrophysics, The University of Chicago, Chicago, IL 60637, USA

<sup>4</sup> Instituto de Investigación Multidisciplinaria en Ciencia y Tecnología, Universidad de La Serena, Raúl Bitrán 1305, La Serena, Chile

<sup>5</sup> Departamento de Astronomía, Universidad de La Serena, Av. Juan Cisternas 1200 Norte, La Serena, Chile

<sup>6</sup> Max-Planck-Institut für Astrophysik, Karl-Schwarzschild-Str. 1, 85748 Garching, Germany

<sup>7</sup> Department of Physics & Astronomy, University of Bologna, via Gobetti 93/2, 40129 Bologna, Italy

Accepted XXX. Received YYY; in original form ZZZ

## ABSTRACT

We use magneto-hydrodynamical simulations of Milky Way-mass haloes from the Auriga project to examine the properties of surviving and destroyed dwarf galaxies that are accreted by these haloes over cosmic time. We show that the *combined* luminosity function of surviving and destroyed dwarfs at infall is similar in the various Auriga haloes, and is dominated by the destroyed dwarfs. There is, however, a strong dependence on infall time: destroyed dwarfs have typically early infall times,  $t_{\text{infall}} < 6$  Gyr, whereas the majority of dwarfs accreted at  $t_{\text{infall}} > 10$  Gyr have survived to the present day. Because of their late infall the surviving satellites today had higher metallicities at infall than their destroyed counterparts of similar infall mass; the difference is even more pronounced for the present-day metallicities of satellites, many of which continue to form stars after infall. In agreement with previous work, we find that a small number of relatively massive destroyed dwarf galaxies dominate the mass of the stellar haloes. However, there is a significant radial dependence: while 90 per cent of the mass in the inner regions ( $< 20$  kpc) is contributed, on average, by only 3 massive progenitors, the outer regions ( $> 100$  kpc) typically have  $\sim 8$  main progenitors of relatively lower mass. Finally, we show that a few massive progenitors dominate the metallicity distribution of accreted stars, even at the metal poor end. Contrary to common assumptions in the literature, dwarf galaxies of mass  $M_{\text{star}} < 10^7 M_{\odot}$  make up less than 10 per cent of the accreted, metal poor stars ( $[\text{Fe}/\text{H}] < -3$ ) in the inner 50 kpc.

**Key words:** Milky Way - Stellar halo - dwarf galaxies - galaxy formation

## 1 INTRODUCTION

The hierarchical nature of galaxy formation in the  $\Lambda$ CDM cosmological paradigm, predicts that galaxies are surrounded by a diffuse stellar halo component, formed by the accretion and disruption of lower mass galaxies (e.g. Bullock & Johnston 2005; Cooper et al. 2010). This formation channel of the stellar halo indicates that it is composed of relatively old, metal poor stars, with substructures associated with various accretion events. The early discovery of the

Sagittarius stream around the Milky Way (Newberg et al. 2002; Majewski et al. 2003), and later on the field of streams (Belokurov et al. 2006), as well as observations of nearby galaxies such as the Andromeda galaxy (McConnachie et al. 2009), are strongly favouring this overall picture of the formation of stellar haloes.

The Galactic halo, which can be resolved into its individual stars and substructures due to proximity, provides a unique window into the past history of the formation of the Milky Way (MW), and allows testing the galaxy formation framework in detail. Recent observational surveys, in particular *Gaia*, are revolutionising our understanding of the

\* E-mail: azadeh.fattahi-savadjani@durham.ac.uk

formation and evolution of our Galaxy and its stellar halo, by providing 6D phase-space information and chemical data on a large number of stars (Gaia Collaboration 2016, 2018). Indeed, the discovery of the Gaia-Sausage-Enceladus population of highly eccentric stars revealed a significant event in the past history of the MW (Belokurov et al. 2018; Haywood et al. 2018; Helmi et al. 2018; Myeong et al. 2018)<sup>1</sup>. This population is thought to be brought in by a relatively massive dwarf galaxy which formed a main component of the inner stellar halo (Fattahi et al. 2019; Mackereth et al. 2019), consistent with predictions from cosmological simulations (Bullock & Johnston 2005; Cooper et al. 2010; Deason et al. 2016).

Early studies comparing chemical properties of the Galactic halo and existing satellites raised questions on whether dwarf galaxies are building blocks of the halo (e.g., Gilmore & Wyse 1998). The lack of extremely metal poor stars in dwarf spheroidal galaxies was part of the tension, which was alleviated later by the discovery of such stars in Sculptor and other dwarfs (Frebel et al. 2010; Starkenburg et al. 2013). Moreover, the difference in the  $[\alpha/\text{Fe}]$  abundance patterns of the stellar halo and dwarf galaxies (see, e.g., Tolstoy et al. 2009; Venn et al. 2004), can be explained by considering that the stellar halo formed from early accretion of relatively more massive dwarf galaxies (Robertson et al. 2005; Font et al. 2006).

The basics of the formation of Galactic haloes were mainly established using N-body cosmological simulations of MW-mass haloes, combined with simple models for the stellar components (such as particle tagging methods; e.g. Bullock & Johnston 2005; Cooper et al. 2010). In particular, these models showed that the mass of Galactic stellar haloes is dominated by few massive dwarf galaxies and the contribution from low mass dwarfs and ultra faint dwarfs is negligible (Deason et al. 2016; Amorisco 2017). High-resolution hydrodynamical simulation suites of MW-mass haloes, where dwarf galaxies that form the stellar halo are resolved, have become accessible in recent year (e.g., APOSTLE, Auriga, Latte, ELVIS; Sawala et al. 2016; Fattahi et al. 2016; Grand et al. 2017; Wetzel et al. 2016; Garrison-Kimmel et al. 2018), allowing more detailed predictions and interpretation of the observational data. These simulations provide the opportunity to follow the formation of stellar haloes in a self-consistent way. Moreover, they offer new features which were not available in N-body simulations, such as gas physics, star formation after infall, self consistent metallicities, and the *in-situ* component of the stellar halo (see below).

Hydrodynamical simulations predict an *in-situ* component to the Galactic stellar halo; i.e. kinematically hot stars which were born in the MW's main progenitor, rather than being accreted. The three main mechanisms for the formation of these stars are: (i) heated disk stars, (ii) stars formed kinematically hot in the halo from cooling gas, (iii) stars formed from the stripped gas from accreted dwarfs (Cooper et al. 2015). The fraction of these stars and the contribution from various formation channels are simulation dependent and are therefore highly debated (see also, Font et al.

<sup>1</sup> Note, however, that it is debated in the literature whether or not Gaia-sausage and Gaia-Enceladus are referring to the same structure and event. See, e.g. Evans (2020).

2011; Pillepich et al. 2018). Indeed, Monachesi et al. (2019) show that the mass of Galactic stellar haloes from the Auriga simulations (Grand et al. 2017) are in better agreement with observations when only the accreted component of the stellar haloes are considered.

In this work, we use the Auriga suite of hydrodynamical simulations of MW-mass haloes, in order to study destroyed dwarf galaxies which formed the accreted Galactic stellar halo, and contrast their properties with those of existing satellites. We additionally examine the radial assembly of stellar haloes and their metallicity content, which are built by the disruption of various dwarf galaxies. This manuscript is organized as the follows. Sec. 2 describes the simulations, followed by comparing the luminosity function, infall time, metallicity and gas content of destroyed and survived satellites in Sec. 3. We present the results on the assembly of Auriga stellar haloes at various radii in Sec. 4, and discuss their metallicity build up in Sec. 4.2. We finally wrap up with a summary in Sec. 5.

## 2 AURIGA SIMULATIONS

In this study we use cosmological, magneto-hydrodynamical (MHD) simulations of MW-mass haloes from the Auriga project (Grand et al. 2017). The Auriga suite consist of ‘zoom-in’ simulations (Power et al. 2003) of relatively isolated haloes with virial mass  $M_{200} \sim 10^{12} M_{\odot}$ , which were chosen from the  $100^3 \text{ Mpc}^3$  periodic box of the EAGLE project (Schaye et al. 2015; Crain et al. 2015). The simulations start at  $z = 127$  from initial conditions which are made by Panphasia (Jenkins 2013), and are developed to  $z = 0$  by the Tree-PM, moving-mesh code, AREPO (Springel 2011; Weinberger et al. 2019). The subgrid galaxy formation model is described in detail in Grand et al. (2017) and Marinacci et al. (2014). In summary, it includes metal line cooling, star formation, stellar evolution feedback (supernovae), supermassive black hole formation and feedback, homogeneous UV photoionizing radiation with re-ionization redshift  $z_{\text{re}} = 6.5$ . The simulations adopt cosmological parameters in accordance to Planck Collaboration (2015):  $\Omega_m = 0.307$ ,  $\Omega_{\Lambda} = 0.693$ ,  $\Omega_{\text{bar}} = 0.048$ , and a Hubble parameter of  $h = 0.6777$ .

We use the original 30 Auriga haloes with halo mass  $M_{200} = (1 - 2) \times 10^{12} M_{\odot}$ , at the fiducial (L4) resolution level with dark matter (baryonic) mass resolution of  $m_{\text{DM}} \sim 3 \times 10^5 M_{\odot}$  ( $m_{\text{bar}} \sim 5 \times 10^4 M_{\odot}$ ), and a maximum Plummer equivalent gravitational softening of  $\epsilon_{\text{max}} = 369$  pc. Six of the Auriga haloes have been simulated at the higher resolution level (L3) with particle mass resolution of  $m_{\text{DM}} \sim 4 \times 10^4 M_{\odot}$  and  $m_{\text{bar}} \sim 6 \times 10^3 M_{\odot}$ , and gravitational softening of  $\epsilon_{\text{max}} = 184$  pc.

Dark matter haloes in the simulations are identified using an FoF algorithm, and bound structures and substructures within FoF groups are found iteratively using SUBFIND (Springel 2005). MW analogs are referred to the central subhalo (subhalo-0) of the main FoF groups, in this work. Grand et al. (2017) present analysis of the galactic disks in the simulations and show that they re-produce the general properties of disk dominated galaxies. Simpson et al. (2018) shows that the luminosity function of the dwarf satellites in Auriga matches that of the Milky Way satellites.

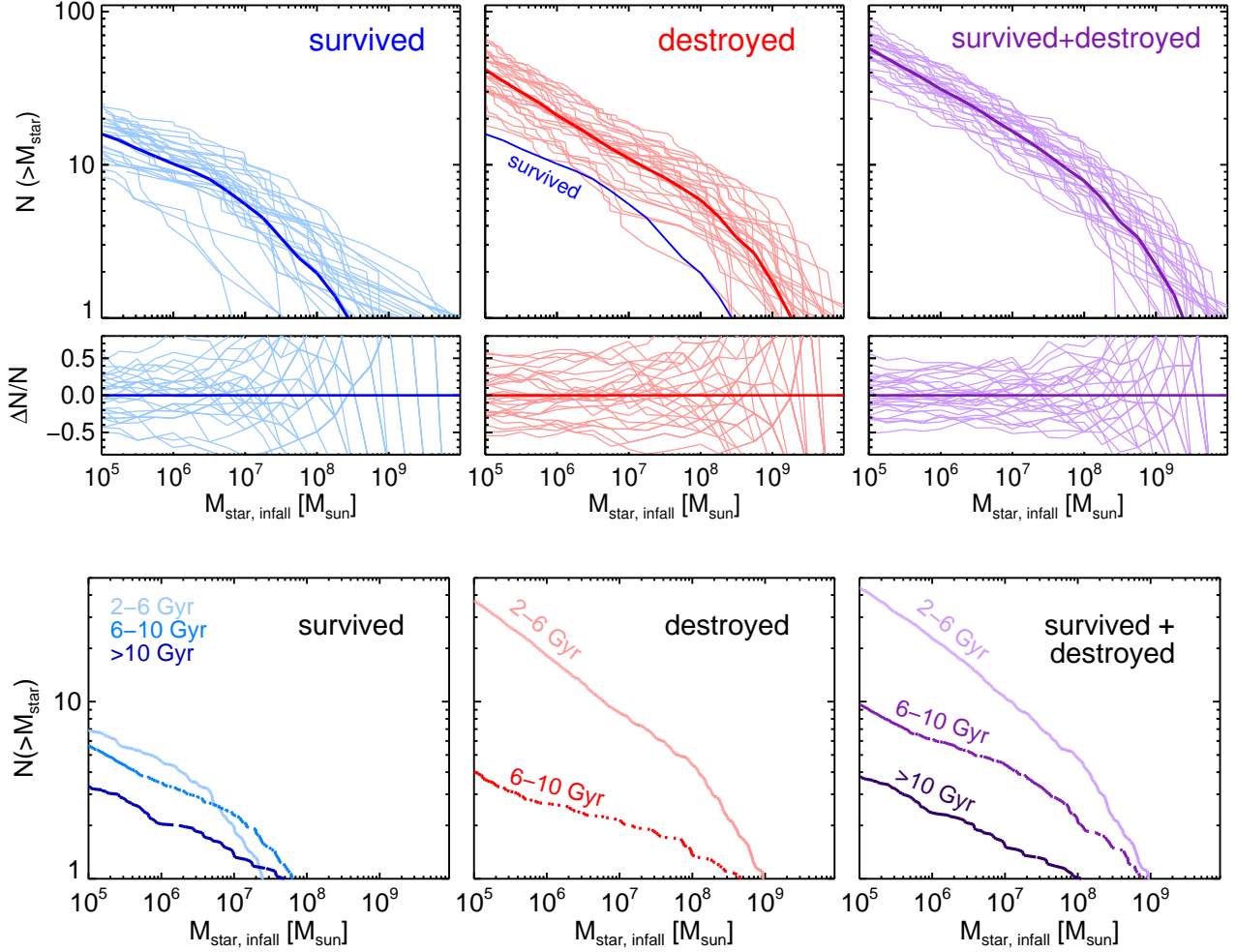


**Figure 1.** Similar to Fig. 1 but stellar mass functions (SMFs) are divided into three infall time bins of  $t_{\text{infall}} = 2-6\text{Gyr}$ ,  $t_{\text{infall}} = 6-10\text{Gyr}$ , and  $t_{\text{infall}} > 10\text{Gyr}$ , as indicated in the legend. The curves represent the average SMF over 28 Auriga haloes. The SMFs strongly depend on infall time, and the typical infall times of the surviving and destroyed populations are very different.

Furthermore, the sizes and star formation histories of the dwarf satellites have also been shown to agree with the observations (Bose et al. 2019; Digby et al. 2019).

In this work, we use merger trees to track galaxies in time only after  $z = 3.1$  ( $t = 2.1\text{ Gyr}$ ), due to the uncertainties in the identification of the main progenitors at earlier time. We refer to destroyed dwarfs as those which have fallen into the main host<sup>2</sup> more recent than  $z = 3.1$  and have no bound remnant (according to SUBFIND) at the present time. For the fiducial resolution (L4), being destroyed is equivalent of galaxy masses falling below  $M_{\text{DM}} \sim 10^7 M_{\odot}$  and  $M_{\text{star}} \sim 10^5 M_{\odot}$ . Satellites are identified as (survived) bound substructures within  $r_{200}$  of the main haloes at  $z = 0$ . Stellar mass and average metallicities of dwarfs at any given time are defined based on bound star particles inside two times their 3D stellar half mass radius ( $r_h$ ). The reference frame of the MW analogs are based on SUBFIND, i.e. the position

of the particle with the minimum gravitational potential. The orientation of galactic disks are defined according to the angular momentum of stars within 10 kpc.

The results presented in this work include 28 Auriga haloes, rather than the full suite of 30, since we discard two of them (Au-11 and Au-20) which are undergoing a merger at  $z = 0$ .

## 2.1 Accreted and in-situ forming stars

In this study, accreted (ex-situ<sup>3</sup>) stars are defined as those which are bound to the MW analogs (i.e. not satellites) at  $z = 0$ , but were bound to a subhalo or halo other than the main progenitor of the MWs, at the snapshot immediately following their birth time. Since we do not track galaxies before  $z = 3.1$  ( $t = 2.1\text{ Gyr}$ ), stars that are formed before that redshift are flagged as accreted or in-situ according to their membership at  $z = 3.1$ . Such old stars make up  $\sim 4$

<sup>2</sup> Infall is defined as crossing the  $r_{200}$  of the main halo for the first time. Infall parameters are based on the snapshot immediately before crossing  $r_{200}$ .

<sup>3</sup> in this work we use the terms ex-situ and accreted interchangeably.

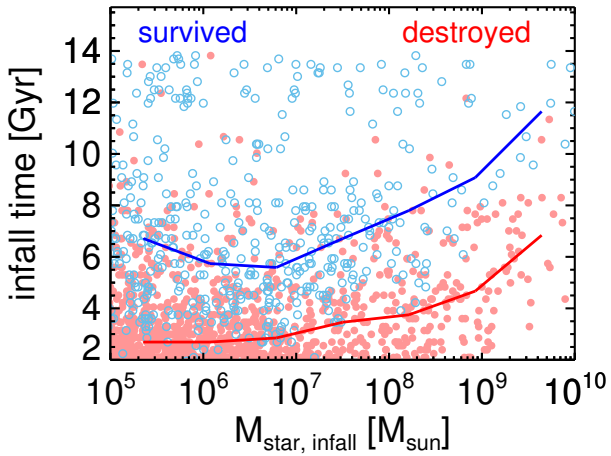


**Figure 2.** Infall time vs. stellar mass at infall for destroyed (red) and surviving dwarfs (blue), accreted onto the 28 Auriga haloes. The curves of similar color show the average infall time at a fixed stellar mass. There is a clear distinction between the infall times of surviving and destroyed dwarfs.

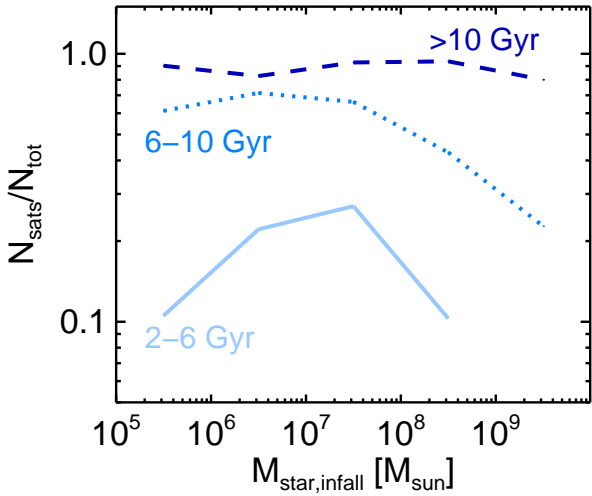


**Figure 3.** Fraction of surviving dwarfs (satellites) relative to all dwarfs that are accreted onto the Auriga haloes, as a function of stellar mass at infall. Different curves correspond to the same infall time bins as in Fig. 1. Almost all dwarfs accreted at late times survive to the present day. At earlier times, the fraction of dwarfs that survives depends on the mass of the dwarf: more massive dwarfs are subject to dynamical friction, and a more rapid destruction, but lower mass dwarfs are more susceptible to tidal effects.

per cent of the final stellar mass in Auriga galaxies, and therefore do not affect our results significantly.

According to our definition of accreted and in-situ stars, stars that are formed in satellite galaxies before and *after* infall are flagged as accreted, while stars that are formed out of stripped gas from satellites (i.e. gas that is not bound to the satellites) are flagged as in-situ. Indeed, most of the gas stripped from satellites gets accreted onto the disk of the galaxy and forms stars there (Cooper et al. 2015).

### 3 DESTROYED VS. SURVIVED DWARF GALAXIES

We present the cumulative stellar mass function (SMF) at infall for surviving satellites<sup>4</sup>, destroyed dwarfs, and the combination of the two populations (i.e. accreted), in the top row of Fig. 1. Lighter color curves correspond to individual haloes, while the thick solid lines show the average of all curves in each panel. This figure includes dwarf galaxies with only a few star particles. Thus, we discuss the convergence of these results using L3 runs in Appendix A, and show that the results are very well converged. We, however, emphasize that the total accreted SMF (right panel) does not suffer from potential numerical artifacts related to tidal stripping and disruption of subhaloes (van den Bosch & Ogiya 2018; Errani & Peñarrubia 2020), since those effects change the relative number of destroyed and survived dwarfs, but not the total number of accreted ones.

This total accreted SMF is the outcome of DM subhalo accretion history combined with the stellar mass-halo mass relation at different redshifts. The former is the pure prediction of the  $\Lambda$ CDM structure formation and has been shown to be relatively similar amongst haloes of similar mass (Jiang & van den Bosch 2015; Guo & White 2008; Ludlow et al. 2013). The stellar mass-halo mass relation depends on the galaxy formation model of the simulations, which have little scatter at the low mass end (Simpson et al. 2018). Therefore, it is not surprising that the *overall* accreted SMF has relatively small scatter amongst various haloes.

Fig. 1 shows that there are fewer satellites, on average, relative to the destroyed dwarfs. However, this does not necessarily imply that the mass of the accreted stellar halo in MW-mass galaxies is larger than the combined stellar mass of the surviving satellites. For example, not all of the accreted mass will end up in the stellar halo; a fraction of mass will end up in the disk and bulge (Gómez et al. 2015). The accreted fraction of bulge is, however, small (Gargiulo et al. 2019). We checked that in these Auriga haloes the median ratio between the total accreted mass inside  $r_{200}$  and the combined stellar mass of the satellites is  $M_{\text{acc}}(< r_{200})/\Sigma M_{\text{sat}} = 3.0$ , with a large scatter of 1.0 dex. This ratio changes to  $M_{\text{acc}}(< r_{200})/\Sigma M_{\text{sat}} = 1.2$  with 0.9 dex scatter when considering the accreted component *outside* of the disk region<sup>5</sup>. Thus, the definition of “stellar halo” is an important consideration when comparing the total mass of accreted components with observations.

#### 3.1 Dependence on Infall time

The SMF of satellites and destroyed dwarfs accreted over cosmic time, have a similar shape (but different normalisation). How does this change as a function of infall time? Fig. 1 presents the SMFs for the same three populations as in the previous figure, but divided into three bins of infall

<sup>4</sup> We use the terms satellites and surviving satellites interchangeably in this work.

<sup>5</sup> Throughout this work, the disk region is loosely defined based on a galactic height cut of  $|z| < 5$  kpc, and cylindrical radius cut of  $R < 20$  kpc.

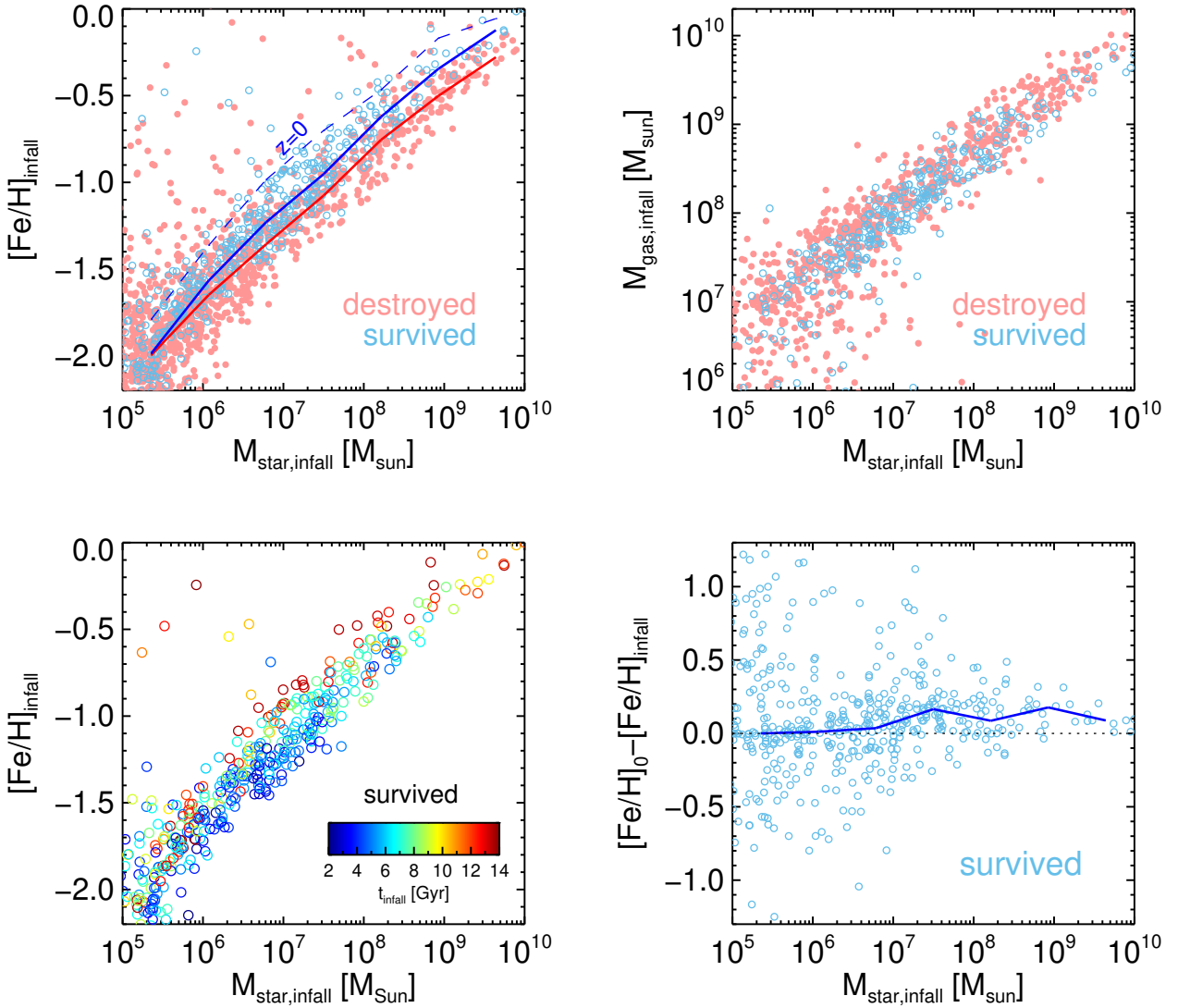


**Figure 4.** Top-left: The average stellar  $[\text{Fe}/\text{H}]$  vs. stellar mass, both at infall, for destroyed (red symbols) and surviving dwarfs (blue symbols). The solid curves show the average  $[\text{Fe}/\text{H}]$  at fixed stellar mass. The dashed line show the average  $M_{\text{star}} - [\text{Fe}/\text{H}]$  relation of satellites at  $z = 0$ . Top-right: Total gaseous mass (inside  $2 \times r_h$ ) vs. stellar mass at infall for destroyed and surviving dwarfs. Colors are similar to the top-left panel. Bottom-left: Similar to top-left, but only for surviving satellites and color coded according to the infall times, indicated by the color bar. Bottom-right: The change in average  $[\text{Fe}/\text{H}]$  between infall and  $z = 0$  for surviving satellites.

time<sup>6</sup> (and averaged over the 28 Auriga haloes). First, it is worth noting the relatively small variations in the SMF of surviving satellites at different infall times, whereas the destroyed population's SMF shows a strong dependence on infall time<sup>7</sup>; in particular, the population is dominated by early infall dwarfs. Additionally, we note that the total accreted dwarfs are dominated, in terms of number and mass, by these early infall dwarfs ( $t_{\text{infall}} = 2 - 6$  Gyr) which are mostly destroyed by the present time.

<sup>6</sup> Infall times throughout this work refer to the age of the Universe when the infall happens, rather than lookback time; i.e.  $t_{\text{infall}} = 0$  is the Big Bang.

<sup>7</sup> Note that only a few destroyed dwarfs over all the haloes, fell in after  $t_{\text{infall}} = 10$  Gyr, hence there is no corresponding line in the middle panel.

The bias in the infall time of the destroyed dwarfs compared to survived satellites, as a function of stellar mass, is shown more clearly in Fig. 2, where circles correspond to individual dwarf galaxies in the 28 Auriga haloes, and the lines represent the average as a function of infall stellar mass. Destroyed dwarfs fell in, on average,  $\sim 5$  Gyr earlier than satellites, with very few ( $\sim 1$  per cent) falling in more recently than  $t = 10$  Gyr; whereas a significant fraction ( $\sim 20$  per cent) of satellites have crossed the virial radius of the host for the first time after  $t = 10$  Gyr. Additionally, we note that the infall times of accreted dwarfs (either destroyed or surviving) increase with stellar mass. This is due to the hierarchical nature of galaxy formation, where more massive galaxies form later from the accretion and mergers of smaller constituents.

The survivability of accreted dwarfs depends both on

their infall time and their infall mass. We examine this in Fig. 3 where we illustrate the fraction of surviving dwarfs to  $z = 0$  relative to the total accreted dwarfs ( $N_{\text{sat}}/(N_{\text{sat}} + N_{\text{destroyed}})$ ), as a function of infall stellar mass, and divided into different infall time bins. The curves show averages over all the 28 haloes. As expected, a large fraction of accreted dwarfs ( $\sim 90$  per cent) which fell in after  $t_{\text{infall}} > 10$  Gyr survive to  $z = 0$ , whereas only 10–20 per cent of the early infall ( $2 < t_{\text{infall}}/\text{Gyr} < 6$ ) dwarfs survive as classical dwarfs ( $M_{\text{star}} > 10^5 M_{\odot}$ ).

There are two interesting points about the trends with stellar mass in Fig. 3. Firstly, more massive objects get destroyed more efficiently. This is well understood to be the result of dynamical friction, which strongly affects more massive objects and drags their orbit towards the centre, and hence leads to more efficient tidal disruption. On the other hand, lower mass objects appear to have a higher chance of getting disrupted. We have checked these results in the L3 runs and confirm that this behaviour persists at higher resolution (see, Fig. A3). Rather than being a resolution artifact, the behaviour at the low mass end can be understood when considering that lower mass objects have lower densities and are less resilient to tides. Interestingly, the combined effects of tides at the low mass end and dynamical friction at the high mass end, result in a mass range,  $M_{\text{star,infall}} \sim 10^7 M_{\odot}$ , where accreted dwarf galaxies have the highest chance of survival (at a fixed infall time).

### 3.2 Metallicity and gas content

The different infall times of the two populations of dwarfs results in differences in the properties of destroyed dwarfs that build up the stellar halo compared to the existing satellites. We examine this in Fig. 4. The top-left panel, which shows  $[\text{Fe}/\text{H}]^8$  vs. stellar mass at infall, indicates that satellites have higher metallicities at infall, compared to their destroyed counterparts of similar  $M_{\text{star,infall}}$ . This is particularly prevalent at higher masses. This can be understood by considering the difference in the infall time of the two populations and the evolution of the stellar mass-metallicity relation with time. We see this in the bottom-left panel, where we show only satellites and color code them according to their infall times. Higher mass satellites fell in, on average, later and formed their stars later from pre-enriched gas. Thus, the later infall times of satellite dwarfs leads them to have more metal-rich stellar populations than their destroyed dwarf counterparts at similar (infall) mass.

All accreted dwarfs, in particular the more massive ones, have a significant amount of gas before infall (Fig. 4); it is therefore not surprising that some dwarfs keep forming stars after infall. The bottom-right panel of Fig. 4 shows that the average metallicities of high mass satellites have increased after infall by roughly 0.2 dex. This is due to their large gas (HI) reservoir, combined with their ability to keep their cold gas for longer after infall and form more stars. Indeed, Simpson et al. (2018) shows that higher mass dwarfs are more resilient to losing their gas due to ram pressure stripping and keep forming stars after infall. At the low mass end, the galaxies do not form many stars after infall, and a

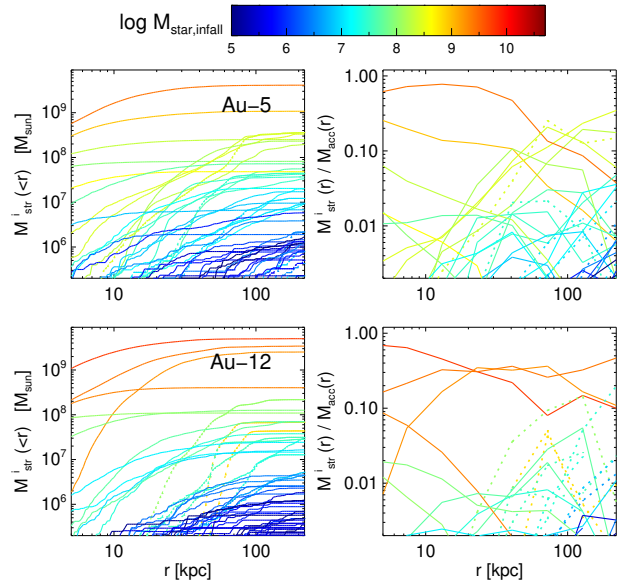


**Figure 5.** The radial distribution of ex-situ stars originated from different progenitor dwarf galaxies, in Auriga halo 5 (top row) and halo 12 (bottom row). Each curve corresponds to star particles associated to a single progenitor and is color coded according to the stellar mass at infall of the progenitor dwarf galaxy. *Left:* Enclosed mass profile of the stars from various progenitors. *Right:* Differential mass fraction (contribution) of stars from various progenitors, relative to the total ex-situ mass, in spherical shells. Massive dwarf progenitors contribute the most stellar mass to the halo, particularly at low radii. However, the contribution from lower mass dwarfs becomes more significant at larger radii.

larger fraction of them are metal poor even before infall (see, Simpson et al. 2018, for details). The decrease in the metallicities of some low mass dwarfs after infall is due to tidal stripping, and the loss of some of the stars. In galaxies with a notable radial gradient in metallicity, tidal stripping is expected to change the average metallicity as less bound, outer stars get stripped first. This effect is less evident in higher mass dwarfs, since the chemical evolution due to star formation after infall dominates. The dashed line in the top left panel shows the average stellar mass-[Fe/H] relation, *both measured at  $z=0$* , for satellites. Indeed, the combination of stellar mass loss (moving left in this panel) and increase of [Fe/H] after infall (moving upward in this panel) enhances the offset between the infall stellar mass-metallicity relation of destroyed dwarf and the  $z=0$  relation for present day satellites.

We emphasize that the low mass end in Fig. 4 suffers from low resolution (i.e. very few star particles); our interpretation should be taken with caution.

Similar to the satellites, destroyed dwarfs would also have formed more stars after infall and before they got fully destroyed, and deposited stars into the stellar halo. We find that these stars (i.e. formed after infall of their progenitor) constitute  $10 \pm 5$  per cent of the mass of the accreted component, where the uncertainty is rms scatter amongst Auriga haloes.

The previous results imply that galactic stellar haloes, which are built up from destroyed dwarfs, are predicted to

<sup>8</sup> Defined as the median metallicity of star particles within  $2 \times r_h$

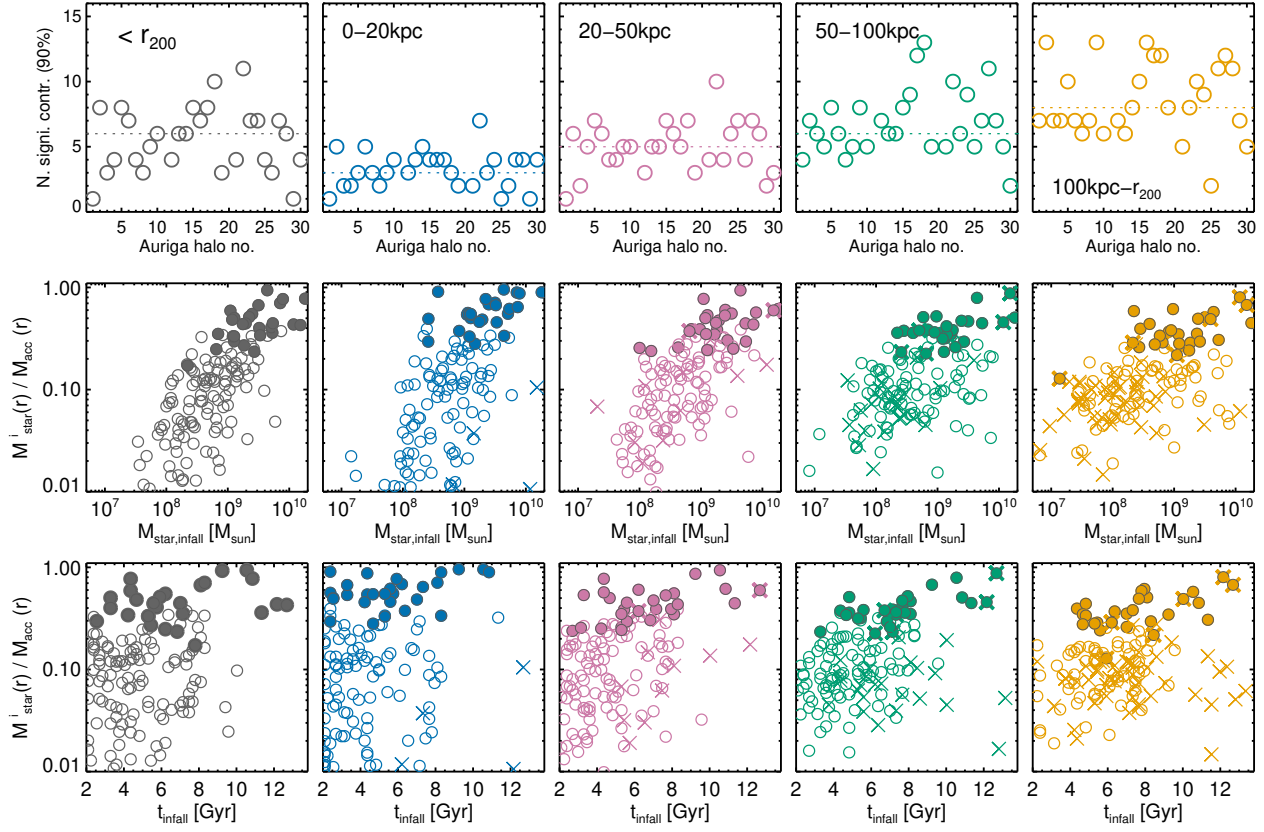


**Figure 6.** *Top row:* The number of significant progenitors at various radial (3D) bins, defined as the main contributors that make up 90 per cent of the ex-situ mass in the given radial range. The left most panel includes all ex-situ stars within  $r_{200}$  of the hosts, while the other panels correspond to various radial bins. *Middle row:* The mass contribution ( $M_i(r)/M_{acc,tot}(r)$ ) of the top 5 progenitors in the given radial range vs. the infall stellar mass of the progenitor dwarf galaxy. Circles and crosses indicates whether the progenitor is destroyed or has survived to  $z = 0$ , respectively. Filled circles highlight the main progenitor of the corresponding radial range, i.e.  $\max(M_i(r)/M_{acc,tot}(r))$  for each Auriga halo. *Bottom row:* Similar to the middle row but showing infall time of the top 5 contributors. The number of significant progenitors increases with radius, and the typical mass of these progenitors decrease with radius. Moreover, the inner regions of the halo are dominated by dwarfs accreted early, while the outer regions comprise of material deposited at later times.

have a different metallicity content than the existing satellites.

#### 4 BUILD-UP OF THE ACCRETED STELLAR HALO

In this Section, we explore how the destroyed dwarf population builds up the accreted stellar halo of Milky Way-mass galaxies.

Fig. 5 shows the stellar mass contribution, as a function of radius, from all progenitors ( $M_{str}$ ) of the stellar halo for two example Auriga galaxies (top and bottom rows). Each solid curve corresponds to an individual destroyed dwarf galaxy, and the dashed curves indicate debris from existing satellites. These lines are all color coded by the progenitors' stellar mass at infall. The enclosed mass profiles (left panels) indicate that more massive dwarf galaxies contribute most to the total mass of the stellar halo within  $r_{200}$ . Moreover, a few massive dwarf galaxies make up most of the mass within  $r_{200}$ , and the mass contribution from numerous low mass dwarfs is very small (see also, Monachesi et al. 2019).

However, right panels of Fig. 5 show that the previous statement does not hold at all radii, and that there is a notable radial dependence. Note that these general trends are seen in all of the Auriga haloes (see Fig. 6). The two examples shown in Fig. 5 are representative for cases where a single dwarf galaxy dominates the build up of the stellar (top row), and where multiple massive dwarf galaxies form most of the halo mass (bottom row).

Both examples in Fig. 5 show that the most massive dwarfs typically deposit most of their stars in the inner regions ( $< \sim 50$  kpc) and their contribution drops in the outer parts, while lower mass dwarf galaxies deposit their stellar mass further out and their contribution only becomes notable at  $r > \sim 50$  kpc. This behaviour is mainly due to dynamical friction, which is a stronger effect for more massive objects and causes their orbits to sink to the centre of the haloes on a relatively short time scale. Therefore more massive objects get tidally stripped and deposit their debris mainly in the inner regions. On the other hand, the orbits of lower mass objects are less affected by dynamical friction, but they are more susceptible to tidal disruption and

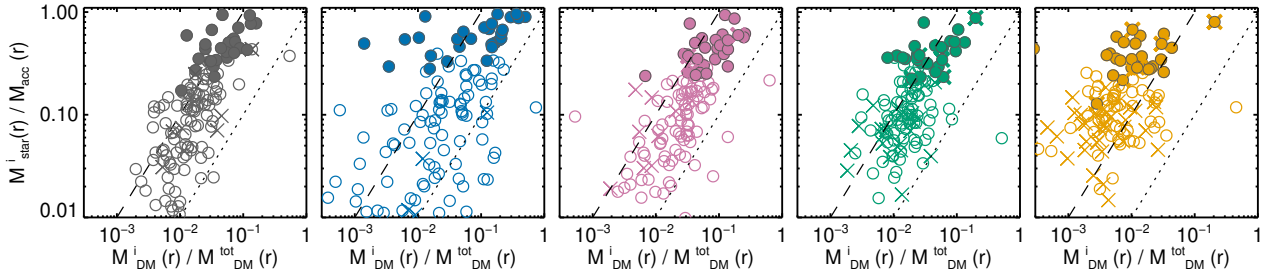


**Figure 7.** The stellar mass contributions from the top 5 progenitors of various radial ranges vs. their DM contribution to the same region. The symbol types and different panels are similar to Fig. 6. Dotted and dashed lines indicate constant 1:1 and 1:10 ratios, respectively. The dark matter contribution from the main progenitors of the stellar halo are typically much smaller than their stellar contribution.

their debris is deposited along their orbits at relatively larger radii.

The next figure (Fig. 6) summarises the previous results, but is now extended to the whole Auriga sample. The top row in Fig. 6 shows the number of significant contributors (progenitors) of the stellar halo at various radii, defined as the top-ranked contributors which formed 90 per cent of the accreted stellar mass in the given radial range. It is clear that the number of significant progenitors increases with radius, amongst all halos; the inner regions ( $< 20$  kpc) are built, on average, from 3 dwarf galaxies, while the outer regions have  $\sim 8$  significant progenitors. The overall number of significant contributors within  $r_{200}$  (left most panel) is 5. The result within  $r_{200}$  is mainly dominated by the properties of the inner regions, as the stellar halo density decreases with radius, and thus most of the mass is in the inner regions.

Do all significant progenitors contribute equally to the stellar halo, and what are they properties? We address these questions in the middle and bottom rows of Fig. 6. Here, we show the top 5 progenitors for each halo at various radii, which are defined as those that have contributed the most stellar mass to the given radial range. As implied earlier, these typically build up 90 per cent of the inner stellar halo.<sup>9</sup>. Circles represent material originated from destroyed dwarf galaxies, and the crosses indicate the debris from existing (survived) dwarfs. The contribution from this latter population is fairly minimal, but becomes more important at larger radii (see below).

The middle row of Fig. 6 shows stellar mass at infall of the progenitors as a function of how much they contributed to the accreted stellar mass in the given radial bin ( $M_{\text{str}}^i(r)/M_{\text{str}}^{\text{acc}}(r)$ ). These panels re-confirm our discussion of the example haloes shown in Fig. 5: the inner regions ( $< 50$  kpc) are strongly dominated by very few relatively massive dwarf galaxies. Filled circles highlight the first progenitor (top contributor) at each radial bin, for all Auriga galaxies. In most Auriga haloes *only one* dwarf galaxy is enough to make up more than  $\sim 50$  per cent of the accreted mass. Moreover, there is a steep correlation between stellar mass of the progenitor dwarf and how much they have contributed to the mass, such that the mass contribution

from dwarf galaxies less massive than  $M_{\text{star}} < 10^8 M_{\odot}$  is negligible (< 1 per cent).

The outer parts of the halo behave differently to the inner regions. In most cases, there is no single progenitor that makes up more than half of the halo, and the contribution from various progenitors become more comparable. It is only in the outer most radial bin ( $> 100$  kpc) that the contribution from  $M_{\text{star}} < 10^8 M_{\odot}$  dwarfs become non-negligible. Additionally, we note that the debris from the surviving dwarfs (crosses) can significantly contribute to the outer parts. On average 12 per cent of the mass in the 100 kpc– $r_{200}$  radial range is contributed from such debris. In comparison, this fraction is negligible in the inner parts. It is worth mentioning that only a small fraction of the total accreted mass is in the outer regions, and the large *fraction* of satellite debris in the outskirts does not mean the majority of this debris mass is in the outer parts.

The bottom row of Fig. 6 is similar to the middle row but shows the infall time of the top 5 progenitors. We can clearly see the inside-out formation of the stellar halo in these panels: the top 5 progenitors of the inner regions typically fell in before  $t_{\text{infall}} = 8$  Gyr, while infall times move towards present day as one considers larger radii. The trend is less clear when one considers only the 1st (i.e. main) progenitors (filled circles). This is because the main progenitors are more massive dwarfs (as can be seen from the middle row), and their mass is relatively dominant at all radii. Moreover, dynamical friction affects their orbits significantly and causes their orbit to sink to the middle regardless of their infall time; hence the existence of late infall ( $t_{\text{infall}} \sim 10$  Gyr) main progenitors in the inner most bin.

#### 4.1 Implications for accreted dark matter

Dwarf galaxies which build up the stellar halo, also contribute to the DM halo of the MW analogs. Owing to the non-linear stellar mass-halo mass relation, and differences in tidal stripping, the DM contribution of these dwarf galaxies are expected to be different from their stellar contribution. For the top 5 contributors to the accreted stellar halo (Fig. 6), Fig. 7 shows their DM mass contribution at various radii ( $M_{\text{dm}}^i(r)/M_{\text{dm}}^{\text{tot}}(r)$ ). This is done by flagging DM particles which were bound to the dwarf galaxy progenitors at infall, and, after disruption of the dwarf galaxy, are now (at  $z = 0$ ) bound to the host.

Generally, the DM contribution of individual dwarfs is

<sup>9</sup> At radii larger than 50 kpc, one could show  $\sim 10$  contributors which make up 90 per cent of the halo; we, however, keep the top 5 contributors to avoiding over-crowded figures.

significantly lower, by almost an order of magnitude, compared to their stellar contributions. These results can be understood by considering that, (i) a considerable fraction of the DM mass is built up by smooth accretion and the disruption of dark subhaloes (Fakhouri & Ma 2010; Genel et al. 2010); and, (ii) the steep shape of the stellar-halo mass relation at the low mass regime (Simpson et al. 2018; Moster et al. 2013; Behroozi et al. 2013) implies that dwarf galaxies over a large range of stellar mass contribute similarly to the DM. Moreover, the results have a larger scatter at various radial bins which is due to the difference in tidal stripping of DM and stars from an accreted dwarf; stars are embedded deeply in the gravitational well of galaxies and are resilient to tides, as opposed to extended DM halos which get stripped first in the outer parts of the halo. In other words, most of the stars from massive dwarfs are deposited in the inner regions while their DM is extended throughout the halo.

#### 4.2 Metallicity of the stellar halo

Lastly, we examine the metallicity contribution of various destroyed dwarf galaxies to the stellar halo. For the results presented in this work,  $[\text{Fe}/\text{H}]$  of stars have been shifted by roughly 0.5 dex so that the median metallicity in the disk matches that measured from SDSS in the solar neighbourhood (see Fattahi et al. 2019, for more details). Fig. 8 illustrates, for two example haloes (the same ones as in Fig. 5), the  $[\text{Fe}/\text{H}]$  distribution of accreted stars in the halo in a spherical shell of  $20 - 50$  kpc. The filled histogram in each panel shows the total distribution, while individual curves correspond to various accreted (and destroyed) dwarf galaxies, color coded based on their stellar mass at infall. These examples demonstrate that the overall distribution is dominated by the most massive dwarfs, particularly at higher metallicities. As the mass of dwarf galaxies decreases, the peak of their  $[\text{Fe}/\text{H}]$  distribution moves towards lower values; a direct consequence of the stellar mass-metallicity relation. However, the lower mass dwarfs never dominate the overall distribution, even at metallicities as low as  $[\text{Fe}/\text{H}] \sim -3$ .

We illustrate this quantitatively in Fig. 9, where we extend the results to all Auriga haloes and various radial ranges. Each panel shows the probability (mass fraction) that accreted stars with  $[\text{Fe}/\text{H}]$  lower than a certain value, given in the legend, are originated from progenitors of various stellar mass. Each panel presents results for four radial ranges. As expected, the higher metallicity bin (i.e.  $[\text{Fe}/\text{H}] < 0$ ) is dominated by massive dwarf galaxies of  $M_{\text{str}}^{\text{infall}} > 10^8 M_{\odot}$ , at all radii. Interestingly, dwarf galaxies below stellar mass of  $M_{\text{str}}^{\text{infall}} < 10^7 M_{\odot}$  only contribute a small fraction, even at the lowest metallicity bin ( $[\text{Fe}/\text{H}] < -3$ ); in particular in the inner most regions which are the most accessible to observations, less than 10 per cent of stars are originated from the lower mass dwarfs. These results have important implications for studies of metal poor stars in the halo, which are often assumed to be tracing the lowest mass dwarfs (Frebel & Norris 2015).

We note that the relative contribution of dwarf galaxies to the stellar halo, in particular the fractions quoted in this section, depend on the stellar-halo mass relation of the simulations and they may change in other models. However, we expect that the overall conclusions will not be affected;

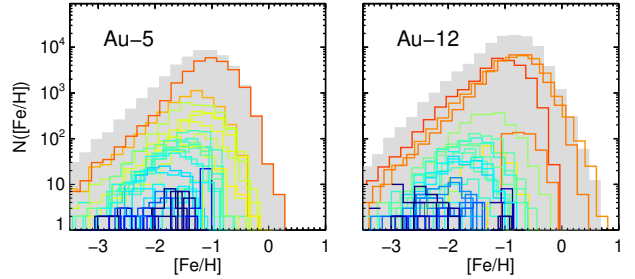


**Figure 8.** The  $[\text{Fe}/\text{H}]$  distribution of accreted stars within the galactocentric distance of  $20 - 50$  kpc, for two Auriga haloes (Au-5 and Au-12 in left and right panels, respectively), subdivided according to their progenitor dwarf galaxy. Distributions are color coded based on the progenitor's stellar mass at infall (color coding is the same as Fig. 5). The total distribution in the  $20 - 50$  kpc radial range is shown as solid histogram in the background. The massive dwarfs dominate the mass fraction of metals contributed to the stellar halo, even at the lowest metallicities.

unless the stellar-halo mass is altered significantly, which would be in contradiction with observational constraints. Other limitations that one should be cautious about concern the lowest metallicity stars. The Auriga simulations do not resolve ultra faint dwarf galaxies and their contribution to the metal poor end of the stellar halo  $[\text{Fe}/\text{H}]$  is thus unknown. We anticipate that their contribution will be small, since their stellar mass is orders of magnitude smaller than the main progenitor of the halo, in particular in the inner halo. A final point to consider is that the Auriga galaxy formation models do not include the formation of first (pop-3) stars, which can affect the shape of the metallicity distribution at the metal poor end.

## 5 SUMMARY AND CONCLUSIONS

We use Auriga magneto-hydrodynamical simulations of 28 MW-mass haloes to study dwarf galaxies that were accreted onto Galactic haloes after  $z \sim 3$  ( $t_{\text{infall}} > 2$  Gyr). We study the population that were destroyed and formed the accreted stellar halo, and contrast their properties with those dwarfs that survived to  $z = 0$  and constitute the satellite population of these haloes. The summary of our findings regarding the properties of these two population are as follows:

- The luminosity function of the total accreted population (destroyed + survived) is similar amongst all Auriga haloes, with little halo-to-halo scatter (0.1 dex scatter around the mean). This reflects the predictable average assembly history of haloes of a given mass in  $\Lambda\text{CDM}$  (Guo & White 2008; Fakhouri et al. 2010; Ludlow et al. 2013), combined with a small scatter (at fixed stellar mass) in the stellar mass-halo mass relation at various redshifts in the simulations.
- The total population of destroyed dwarf galaxies are dominant over surviving satellites by both number and mass. Averaged over all halos, 28 (33) per cent of accreted dwarfs with infall stellar mass of  $M_{\text{star}} > 10^5 M_{\odot}$  ( $M_{\text{star}} > 10^7 M_{\odot}$ ) survive to  $z = 0$ . This indicates that ex-situ stellar mass of the halo is typically larger than the combined mass of the satellites. However, we find that the ex-situ stellar mass within the virial radius and outside of the Galactic disk

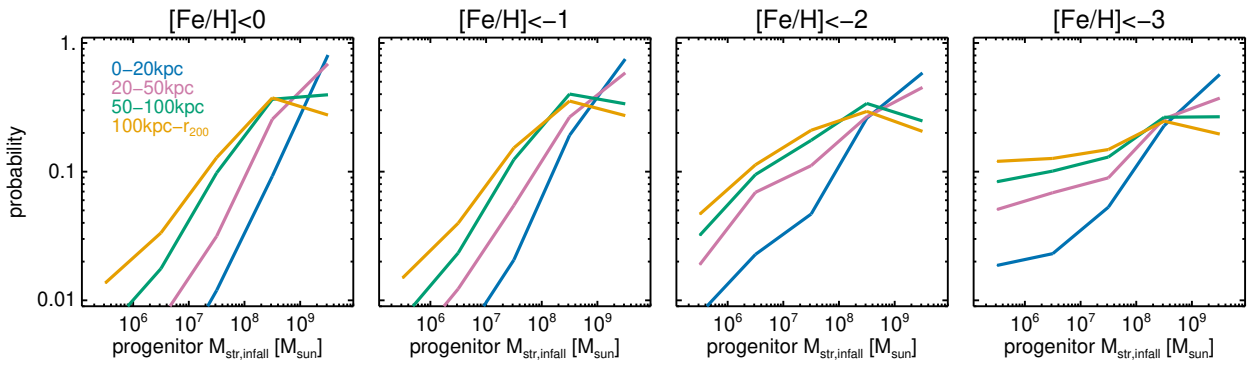


**Figure 9.** The probability (given by mass fraction) that accreted stars at a given metallicity originated from progenitors of different stellar mass. The various panels correspond to different  $[\text{Fe}/\text{H}]$  cuts, as stated in the legends, and lines of different color correspond to different radial ranges. Even at the lowest metallicities ( $[\text{Fe}/\text{H}] < -3$ ), the most likely contributors to the accreted stars are the most massive dwarfs.

region of the Auriga galaxies is, on average, comparable (mass ratio 1.2) to the total stellar mass bound to existing satellites. This is mainly because a significant amount of destroyed dwarf debris is deposited into the very central regions of the halo.

- The fraction of surviving dwarf galaxies is strongly dependent on the infall time, as well as the mass at infall. Roughly 90 per cent of dwarfs that were accreted after  $t_{\text{infall}} = 10$  Gyr survive to present day, and this fraction drops to only 15 per cent for early accretion events ( $t_{\text{infall}} = 2 - 6$  Gyr). The survival fraction also depends on the mass at infall, such that both high mass and low mass dwarfs are destroyed more efficiently, while accreted dwarfs with  $M_{\text{star,infall}} \sim 10^7 M_{\odot}$  are the most resilient. Dynamical friction is responsible for the efficient destruction of higher mass dwarfs, while lower mass objects are less resilient to mass loss due to tidal stripping.

- The average infall time of satellites (surviving dwarfs) is  $\sim 7$  Gyr, with a dependence on the mass at infall. For example, the typical infall time is  $\sim 6$  Gyr and  $\sim 10$  Gyr for satellites with infall stellar mass of  $10^6 M_{\odot}$  and  $10^9 M_{\odot}$ , respectively. In contrast, destroyed dwarfs have an average infall time of  $t_{\text{infall}} \sim 2.5$  and  $\sim 5$  Gyr for stellar mass of  $M_{\text{star,infall}} \sim 10^6$  and  $10^9 M_{\odot}$ , respectively. The increase in the infall time of accreted dwarfs with increasing mass is a consequence of hierarchical formation of galaxies; higher mass galaxies form later from smaller galaxies.

- Due to the slight evolution of the stellar mass-metallicity relation with time, the later infall time of satellites implies that their metallicity ( $[\text{Fe}/\text{H}]$ ) at infall is higher than their destroyed counterparts of similar stellar mass. This difference is 0.2 dex at stellar mass of  $M_{\text{star,infall}} \sim 10^8 - 10^9 M_{\odot}$ . The higher mass satellites are gas rich at infall and continue star forming after infall, causing their  $[\text{Fe}/\text{H}]$  to increase further by 0.2 dex to the present day. These results imply that the metallicity of the stellar halo (which is formed from the destroyed dwarfs) is lower than the existing satellites, which is consistent with observations of the MW and Andromeda system (Vargas et al. 2014).

In the second half of the paper, we focus on the material deposited from destroyed (and disrupted) dwarfs in Auriga galaxies and the assembly of their accreted stellar haloes.

These results are complementary to those of Monachesi et al. (2019). We extend the results of that work by examining progenitors of the accreted stellar halo at various radii. We also study some additional parameters, such as the DM and metallicity contribution of the destroyed dwarfs. Our results concerning the overall halo are consistent with the finding of Monachesi et al. (2019).

We identified all stars that formed later than  $z = 3$  ( $t = 2$  Gyr) in progenitors which are not the main progenitor of the MW, but are bound to the MW analogs at  $z = 0$ . On average 15 per cent of these stars end up in the inner 5 kpc ( $\sim$  bulge region), and 50 per cent in the disk region ( $R < 10$  kpc and  $|z| < 5$  kpc). Our results concerning all these ex-situ components are summarized below.

- In agreement with previous studies, we find that the total accreted mass of the stellar halo within  $r_{200}$  is assembled by a few relatively massive dwarf galaxies. We, however, show that this statement varies as a function of galactocentric radius ( $r_{\text{GC}}$ ). The inner most regions, i.e.  $r_{\text{GC}} < 20$  kpc, have typically  $\sim 3$  significant dwarf progenitors which make up 90 per cent of the mass, and this number changes to 5 and 8 for  $r_{\text{GC}} = 20 - 50$  kpc and  $r_{\text{GC}} > 50$  kpc regions, respectively. In the inner 20 kpc, the contribution of individual dwarfs drops rapidly with the mass of the progenitor dwarf galaxy, such that more than 50 per cent of the mass is typically coming from one single massive dwarf galaxy, and the contribution of dwarf galaxies with mass lower than  $M_{\text{star}} < 10^8 M_{\odot}$  is negligible. In the outer regions, however, the contribution from various progenitors are more comparable. The recent discovery of the *Gaia-sausage-Enceladus* (Helmi et al. 2018; Belokurov et al. 2018) from *Gaia* data is in agreement with our findings. Indeed, this merger is thought to dominate the mass of the Galactic inner stellar halo.

- The contribution of debris from existing satellites is significant in the outer regions of the stellar haloes. On average,  $\sim 30 \pm 25$  per cent of the ex-situ mass in the  $r_{\text{GC}} = 100\text{kpc} - r_{200}$  spherical shell is made up of such stars. This fraction is much smaller,  $< 1$  per cent, in the inner 20 kpc region.

- The significant contributions of more massive dwarf galaxies to the galactic stellar haloes have important im-

plications for the metallicity content of the halo. Unsurprisingly, more massive (destroyed) dwarfs are the main origin of higher metallicity ( $[\text{Fe}/\text{H}] \sim (-1, 0)$ ) stars. However, we find that even at the more metal poor tail of the distribution, stars originated from low mass dwarf galaxies do not dominate. In the inner 20 kpc, stars more metal poor than  $[\text{Fe}/\text{H}] < -3$  have less than 10 per cent chance, on average, of being deposited from dwarf galaxies with lower mass than  $10^7 M_\odot$ . This finding is an important consideration for the interpretation of results from surveys such as Pristine (Starkenburg et al. 2017), which target metal poor stars (e.g. Sestito et al. 2020; Youakim et al. 2020).

- We show that the accreted stellar haloes are formed inside-out; i.e. the top progenitors of the inner stellar haloes have infall time typically less than  $t_{\text{infall}} < 6 \text{Gyr}$ , whereas the top progenitors of the outer parts have more recent infall times.

- We show that the build up of the stellar halo is significantly different from that of the dark matter. The dark matter contribution of the stellar halo progenitors is typically an order of magnitude lower than their stellar contribution. Moreover, their stellar mass vs dark matter contribution various as a function of radius. These findings are the result of the steep shape of the stellar mass-halo mass relation at the low mass end (dwarf galaxies of various stellar mass, live in similar halo masses), and the fact that a significant fraction of dark matter halo mass is built up from dark subhaloes and smooth accretion. In addition, the difference in the tidal stripping of dark matter vs. stars from accreted dwarf galaxies results in differences at various radii. Dark matter is typically stripped first and deposited at larger radii, as opposed to the stars which are deeply embedded in the potential well of dwarfs and get disrupted last, close to pericentre.

Our findings regarding both surviving satellites and destroyed dwarf galaxies indicate that the observed satellites at present day are *not* the building blocks of the stellar halo. The building blocks of the stellar halo are a biased population of dwarf galaxies which fell in relatively early, and differ from observed satellites, in particular in their metallicity content. Moreover, the observed satellites are dominated in number by low mass dwarfs, whereas low mass dwarf galaxies contribute negligibly to the mass of the inner stellar halo, even at low metallicities. This implies that the kinematic properties of the metal poor stars is biased, and differs from what is expected from the accretion of numerous dwarf galaxies with various orbital parameters. This will be the subject of a future work.

## ACKNOWLEDGEMENTS

AF is supported by an Marie-Curie COFUND/Durham Junior Research Fellowship (under EU grant agreement no. 609412), and AD by a Royal Society University Research Fellowship. AD, AF and CSF are also supported by the Science and Technology Facilities Council (STFC) [grant numbers ST/F001166/1, ST/I00162X/1, ST/P000541/1]. CSF is also supported by ERC Advanced Investigator grant, DMIDAS [GA 786910]. FM acknowledges support through the Program ‘Rita Levi Montalcini’ of the Italian MIUR. AM

acknowledges financial support from CONICYT FONDECYT Regular 1181797. FAG acknowledges financial support from CONICYT through the project FONDECYT Regular Nr. 1181264. FAG and AM acknowledge funding from the Max Planck Society through a Partner Group grant.

This work used the DiRAC Data Centric system at Durham University, operated by the ICC on behalf of the STFC DiRAC HPC Facility ([www.dirac.ac.uk](http://www.dirac.ac.uk)). This equipment was funded by BIS National E-infrastructure capital grant ST/K00042X/1, STFC capital grant ST/H008519/1, and STFC DiRAC Operations grant ST/K003267/1 and Durham University. DiRAC is part of the National E-Infrastructure.

## REFERENCES

Amorisco N. C., 2017, *MNRAS*, **464**, 2882  
 Behroozi P. S., Marchesini D., Wechsler R. H., Muzzin A., Papovich C., Stefanon M., 2013, *ApJ*, **777**, L10  
 Belokurov V., et al., 2006, *ApJ*, **642**, L137  
 Belokurov V., Erkal D., Evans N. W., Koposov S. E., Deason A. J., 2018, *MNRAS*, **478**, 611  
 Bose S., et al., 2019, *MNRAS*, **486**, 4790  
 Bullock J. S., Johnston K. V., 2005, *ApJ*, **635**, 931  
 Cooper A. P., et al., 2010, *MNRAS*, **406**, 744  
 Cooper A. P., Parry O. H., Lowing B., Cole S., Frenk C., 2015, *MNRAS*, **454**, 3185  
 Crain R. A., et al., 2015, *MNRAS*, **450**, 1937  
 Deason A. J., Mao Y.-Y., Wechsler R. H., 2016, *ApJ*, **821**, 5  
 Digby R., et al., 2019, *MNRAS*, **485**, 5423  
 Errani R., Peñarrubia J., 2020, *MNRAS*, **491**, 4591  
 Evans N. W., 2020, arXiv e-prints, p. [arXiv:2002.05740](https://arxiv.org/abs/2002.05740)  
 Fakhouri O., Ma C.-P., 2010, *MNRAS*, **401**, 2245  
 Fakhouri O., Ma C.-P., Boylan-Kolchin M., 2010, *MNRAS*, **406**, 2267  
 Fattahi A., et al., 2016, *MNRAS*, **457**, 844  
 Fattahi A., et al., 2019, *MNRAS*, **484**, 4471  
 Font A. S., Johnston K. V., Bullock J. S., Robertson B. E., 2006, *ApJ*, **638**, 585  
 Font A. S., McCarthy I. G., Crain R. A., Theuns T., Schaye J., Wiersma R. P. C., Dalla Vecchia C., 2011, *MNRAS*, **416**, 2802  
 Frebel A., Norris J. E., 2015, *ARA&A*, **53**, 631  
 Frebel A., Kirby E. N., Simon J. D., 2010, *Nature*, **464**, 72  
 Gaia Collaboration 2016, *A&A*, **595**, A2  
 Gaia Collaboration 2018, *A&A*, **616**, A1  
 Gargiulo I. D., et al., 2019, *MNRAS*, **489**, 5742  
 Garrison-Kimmel S., et al., 2018, arXiv e-prints,  
 Genel S., Bouché N., Naab T., Sternberg A., Genzel R., 2010, *ApJ*, **719**, 229  
 Gilmore G., Wyse R. F. G., 1998, *AJ*, **116**, 748  
 Gómez F. A., Besla G., Carpentero D. D., Villalobos Á., Orsquia oShea B. W., Bell E. F., 2015, *ApJ*, **802**, 128  
 Grand R. J. J., et al., 2017, *MNRAS*, **467**, 179  
 Guo Q., White S. D. M., 2008, *MNRAS*, **384**, 2  
 Haywood M., Di Matteo P., Lehnert M. D., Snaith O., Khoperskov S., Gómez A., 2018, *ApJ*, **863**, 113  
 Helmi A., Babusiaux C., Koppelman H. H., Massari D., Veljanoski J., Brown A. G. A., 2018, *Nature*, **563**, 85  
 Jenkins A., 2013, *MNRAS*, **434**, 2094  
 Jiang F., van den Bosch F. C., 2015, *MNRAS*, **453**, 3575  
 Ludlow A. D., et al., 2013, *MNRAS*, **432**, 1103  
 Mackereth J. T., et al., 2019, *MNRAS*, **482**, 3426  
 Majewski S. R., Skrutskie M. F., Weinberg M. D., Ostheimer J. C., 2003, *ApJ*, **599**, 1082  
 Marinacci F., Pakmor R., Springel V., 2014, *MNRAS*, **437**, 1750  
 McConnachie et al. 2009, *Nature*, **461**, 66

Monachesi A., et al., 2019, *MNRAS*, **485**, 2589

Moster B. P., Naab T., White S. D. M., 2013, *MNRAS*, **428**, 3121

Myeong G. C., Evans N. W., Belokurov V., Sanders J. L., Koposov S. E., 2018, *ApJ*, **863**, L28

Newberg H. J., et al., 2002, *ApJ*, **569**, 245

Pillepich A., et al., 2018, *MNRAS*, **475**, 648

Planck Collaboration 2015, preprint, ([arXiv:1502.01589](https://arxiv.org/abs/1502.01589))

Power C., Navarro J. F., Jenkins A., Frenk C. S., White S. D. M., Springel V., Stadel J., Quinn T., 2003, *MNRAS*, **338**, 14

Robertson B., Bullock J. S., Font A. S., Johnston K. V., Hernquist L., 2005, *ApJ*, **632**, 872

Sawala T., et al., 2016, *MNRAS*, **457**, 1931

Schaye J., et al., 2015, *MNRAS*, **446**, 521

Sestito F., et al., 2020, *MNRAS*,

Simpson C. M., Grand R. J. J., Gómez F. A., Marinacci F., Pakmor R., Springel V., Campbell D. J. R., Frenk C. S., 2018, *MNRAS*, **478**, 548

Springel V., 2005, *MNRAS*, **364**, 1105

Springel V., 2011, arXiv e-prints, p. [arXiv:1109.2218](https://arxiv.org/abs/1109.2218)

Starkenburg E., et al., 2013, *A&A*, **549**, A88

Starkenburg E., et al., 2017, *MNRAS*, **471**, 2587

Tolstoy E., Hill V., Tosi M., 2009, *ARA&A*, **47**, 371

Vargas L. C., Geha M. C., Tollerud E. J., 2014, *ApJ*, **790**, 73

Venn K. A., Irwin M., Shetrone M. D., Tout C. A., Hill V., Tolstoy E., 2004, *AJ*, **128**, 1177

Weinberger R., Springel V., Pakmor R., 2019, arXiv e-prints, p. [arXiv:1909.04667](https://arxiv.org/abs/1909.04667)

Wetzel A. R., Hopkins P. F., Kim J.-h., Faucher-Giguère C.-A., Kereš D., Quataert E., 2016, *ApJ*, **827**, L23

Youakim K., et al., 2020, *MNRAS*, **492**, 4986

van den Bosch F. C., Ogiya G., 2018, *MNRAS*, **475**, 4066

## APPENDIX A: CONVERGENCE

We show the convergence between L4 and L3 Auriga runs in Fig. A1, A2, and A3 which are equivalents of Fig. 1, 2, and 3 in the main text, respectively. These results include only the 6 haloes that were run at both resolutions.

The luminosity function of the total accreted population (right panel of Fig. A1) shows an excellent convergence between the two resolution runs. However, we note that  $\sim 10$  per cent of dwarfs have moved from the destroyed population to the surviving one.

The definition of “destroyed” in the L3 results presented here are equivalent to the L4 resolution: halo mass less than  $10^7 M_\odot$  or  $M_{\text{star}} < 10^5 M_\odot$ . We tried relaxing this definition to include any accreted dwarf which got completely destroyed by  $z = 0$ , and the result did not change in any meaningful way. We note that dwarf galaxies form in relatively massive, well-resolved haloes ( $10^9 - 10^{10} M_\odot$  halos or  $10^4 - 10^5$  number of particles in L4), not in haloes at the resolution limit.

As implied from Fig. A1, dwarf galaxies in the higher resolution runs have a  $\sim 10$  per cent higher chance of surviving. This is independent of stellar mass, and indicates that the down turn in the surviving fraction at lower masses is not a resolution dependent effect.

This paper has been typeset from a TeX/LaTeX file prepared by the author.

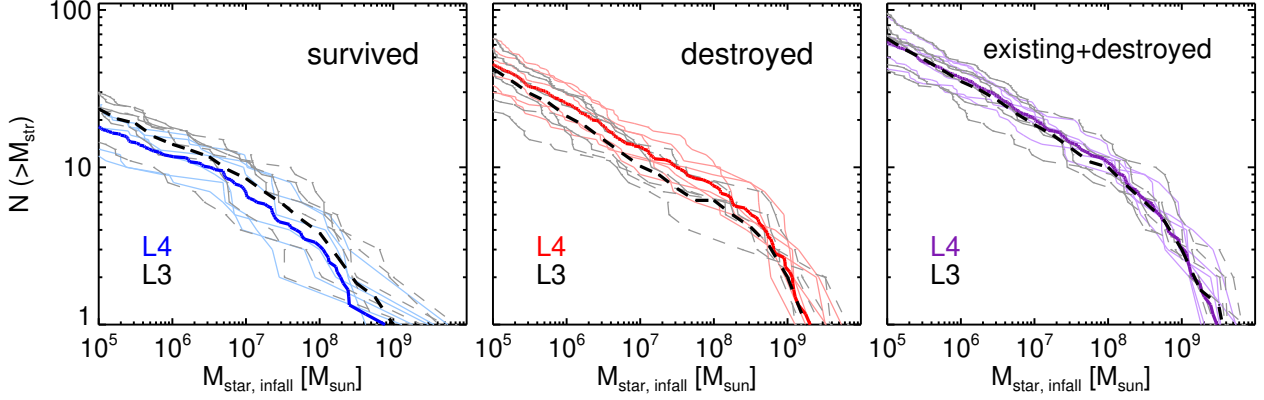


**Figure A1.** Similar to Fig. 1 but showing the convergence between higher resolution (L3) runs and the fiducial resolution used in this work (L4). This figure considers only the 6 haloes which have both L3 and L4 runs. The grey and black curves correspond to L3 results, while colored lines show L4 results.

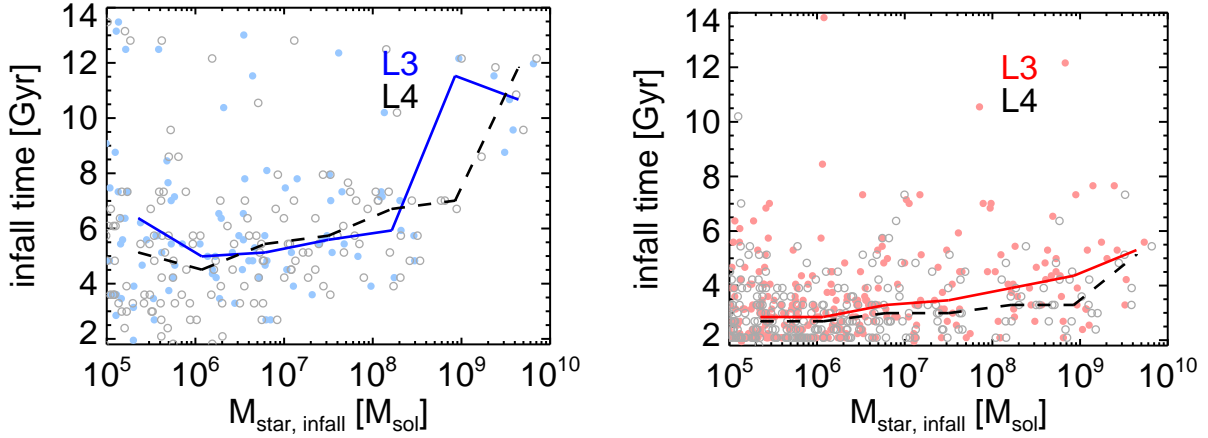


**Figure A2.** Similar to Fig. 2 but divided into surviving dwarfs and destroyed dwarfs in the left and right panels, respectively. Small grey and colored symbols illustrate individual dwarfs at L3 and L4 runs, respectively. Similarly, black and colored curves show the average for the two resolutions.

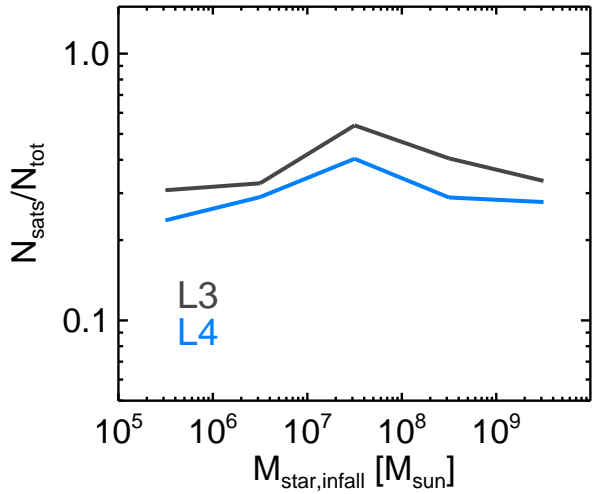


**Figure A3.** The fraction of surviving dwarfs (satellites), relative to all accreted dwarfs, as a function of stellar mass at infall, for six Auriga haloes at resolution levels L3 and L4. Due to the low number of dwarfs, we did not divide dwarfs into various infall time bins.